



HAL
open science

Discrimination and concentration measurement of different binary gas mixtures with a simple resonator through viscosity and mass density measurements

L. Iglesias, M.T. Boudjiet, I. Dufour

► **To cite this version:**

L. Iglesias, M.T. Boudjiet, I. Dufour. Discrimination and concentration measurement of different binary gas mixtures with a simple resonator through viscosity and mass density measurements. *Sensors and Actuators B: Chemical*, 2019, 285, pp.487-494. hal-02013279

HAL Id: hal-02013279

<https://hal.science/hal-02013279>

Submitted on 21 Oct 2021

HAL is a multi-disciplinary open access archive for the deposit and dissemination of scientific research documents, whether they are published or not. The documents may come from teaching and research institutions in France or abroad, or from public or private research centers.

L'archive ouverte pluridisciplinaire **HAL**, est destinée au dépôt et à la diffusion de documents scientifiques de niveau recherche, publiés ou non, émanant des établissements d'enseignement et de recherche français ou étrangers, des laboratoires publics ou privés.



Distributed under a Creative Commons Attribution - NonCommercial 4.0 International License

Discrimination and Concentration Measurement of Different Binary Gas Mixtures with a Simple Resonator through Viscosity and Mass Density Measurements

L. Iglesias, M.T. Boudjiet, I. Dufour*

Univ. Bordeaux, IMS, UMR 5218, F-33400 Talence, France

Abstract

Compared to physical microsensors based on the measurement of physical properties of gases, chemical microsensors are attractive for detection of gas due to their selectivity and relatively high sensitivity. However, most of the time they present a considerable drift in their output which either requires recalibration or makes them unsuitable for several applications. Physical gas microsensors used for chemical detection on the other hand lack of selectivity which makes them unsuitable for applications where more than one gas concentration is susceptible to change. In this paper, a new method is exposed, that allows physical microsensors to discriminate different binary gas mixtures in applications such as industrial gas monitoring, where the viscosity and mass density of the gases prone to manifest are known. The method is based on the measurement of both the resonant frequency and the quality factor in microresonators. The small variations of such signals are interpreted in terms of viscosity and mass density variations with respect to a reference gas such as nitrogen (N_2). This method allows the discrimination of the gases mixtures as well as the determination of the gas concentration.

Keywords: Gas Sensing, Gas Discrimination, MEMS, Viscosity, Density, Uncoated Cantilever

1. Introduction

Stability and long time reliability are two well known limitations regarding chemical gas micro sensors [1, 2, 3]. Although metal oxide based (MOX) sensors, according to Romain *et al.* [2, 3], have relatively good stability, they typically require either a recalibration, or to be replaced after a few weeks or a couple of months due for instance to aging [4] of the sensitive film. A lot of effort has been put into making chemical sensors more stable over time such as improving the materials used [5, 6]. Some researchers even proposed to apply statistical models [7] or even machine learning algorithms like support vector machines [8] and artificial neural networks [9] to compensate for the drift. This, naturally, requires a fairly important amount of computation and processing. Another approach is to simply not use a sensitive film at all which has resulted in an increasing interest towards using uncoated resonators for chemical detection [10, 11, 12, 13]. Tétin *et al.* [11] showed that the shift in the resonant frequency of an uncoated cantilever can be associated to both the density and the viscosity of its surrounding fluid. This allowed for measurements of molar fractions for several gases such as carbon dioxide (CO_2) [11] and hydrogen (H_2) [12, 13].

Nevertheless, one of the difficulties of this approach is the lack of selectivity resulting from removing the sensor's sensitive film which strongly limits its applications. Indeed, every chemical specie is susceptible of changing the physical properties of the sensor environment which makes it difficult to differentiate between different species.

*Corresponding author

Email address: isabelle.dufour@ims-bordeaux.fr (I. Dufour)

Nonetheless, as presented in [Table 1](#), measuring particular properties of the surrounding gas such as viscosity (η) or mass density (ρ) is most certainly a first step towards discriminating different chemical entities. The physical properties of some common industrial gases can vary considerably from one gas to another. Although in the following parts we will focus on measuring both the viscosity and the mass density; the thermal conductivity and the speed of sound could potentially improve the uniqueness of a gas signature to identify it. There exist several ways to measure a fluid's viscosity and mass density simultaneously [14, 15, 16, 17] although very often it consists of a system of two sensors such as a flow and a pressure sensor. Integrated versions are rare but they can be found in the literature[16]. Resonators also have been used to measure both mass density and viscosity [14] but due to the small viscosity of gases at atmospheric pressure some techniques are useful for liquids only. Despite this challenge Lötters *et al.* managed to measure simultaneously density, viscosity, heat capacity and mass flow of several gases included H_2 by integrating a pressure, a thermal and a Coriolis microsensors [16]. In this article we present a method that not only can measure both quantities from a single microresonator for a given gas mixture, but it can also discriminate from different binary gas mixtures and estimate the gas concentration.

In this paper the idea of using both the viscosity and the mass density of a binary gas mixture to discriminate different gases and to estimate their concentration is presented ([Section 2](#)). Then the method to determine both the viscosity and the mass density of a gas from the measurement of both the resonant frequency and the quality factor of an uncoated microresonator is exposed ([Section 3](#)). The silicon microcantilever and the measurement equipments used to test the proposed method are presented in [Section 4](#) and the obtained results are presented in [Section 5](#). Finally, because the method used a calibration step, the impact of the choice of gases and concentrations for the calibration is studied ([Section 6](#)).

2. Motivation

[Figure 1](#) shows the theoretical mass density difference ($\Delta\rho$) against the theoretical viscosity difference ($\Delta\eta$), both with respect to nitrogen, for different molar fractions in percent and for different gases.

The mixture mass density was computed using [Equation 1](#) which comes from the definition of the mass density:

$$\rho_{G-N_2} = \rho_G x_G + (1 - x_G)\rho_{N_2}, \quad (1)$$

where x_G , ρ_G , ρ_{N_2} and ρ_{G-N_2} are the molar fraction of the gas, G , present in a small amount, its mass density, the mass density of nitrogen and the one of the mixture, respectively.

The mixture viscosity was computed using the approximated equation from the kinetic gas theory [18, 19, 20]:

$$\eta_{G-N_2} = \frac{x_G \eta_G}{x_G + (1 - x_G)\Phi_{G-N_2}} + \frac{(1 - x_G)\eta_{N_2}}{1 + (\Phi_{N_2-G} - 1)x_G}, \quad (2)$$

where η_G , η_{N_2} and η_{G-N_2} refer to the viscosity of the gas present in a small amount, nitrogen and the mixture, respectively. Φ_{G-N_2} and Φ_{N_2-G} are given in [Equations 3](#) and 4, respectively.

$$\Phi_{G-N_2} = \frac{[1 + (\frac{\eta_G}{\eta_{N_2}})^{\frac{1}{2}} (\frac{M_{N_2}}{M_G})^{\frac{1}{4}}]^2}{[8(1 + \frac{M_G}{M_{N_2}})]^{\frac{1}{2}}}, \quad (3)$$

$$\Phi_{N_2-G} = \frac{[1 + (\frac{\eta_{N_2}}{\eta_G})^{\frac{1}{2}} (\frac{M_G}{M_{N_2}})^{\frac{1}{4}}]^2}{[8(1 + \frac{M_{N_2}}{M_G})]^{\frac{1}{2}}}, \quad (4)$$

where M_{N_2} and M_G are the molar weight of nitrogen and of the gas present in a small amount, respectively.

It can be noticed that in [Figure 1](#) some gases with similar mass density variations for a given molar fraction such as hydrogen and helium can differ considerably in their viscosity variation. Similarly, gases with close viscosity variations for a given molar fraction such as oxygen and helium can be differentiated by their mass density variations. There is, however, an additional advantage of measuring both variables

$\Delta\rho$ and $\Delta\eta$. As illustrated in Figure 1 and Table 2, the slope of the curves of Figure 1 ($\frac{\eta_{N_2}}{\rho_{N_2}} \frac{\Delta\rho}{\Delta\eta}$) is a good parameter to discriminate between different gases. Finally, once the gas mixture is determined, its molar fraction is given either by $\Delta\rho$ or $\Delta\eta$ depending on which signal is easier to detect. For instance, as shown in Table 2, the sensitivity to mass density ($\frac{\Delta\rho}{x_G \rho_{N_2}}$) for H_2 is much higher than the one to viscosity ($\frac{\Delta\eta}{x_G \eta_{N_2}}$).

3. Model

In Sader's theory [21, 22], in the case of a beam respecting Euler-Bernoulli conditions ($L \gg b \gg h$ where L , b , and h are the length, width and thickness of the cantilever, respectively), it has been shown [11] that for small variations $\Delta\rho$ and $\Delta\eta$ of mass density and viscosity respectively, these quantities are related to the shift in resonant frequency Δf_r as described by Equation 5.

$$\frac{\Delta f_r}{f_r} = -\frac{\pi}{8} \frac{\rho}{\rho_{beam}} \frac{b}{h} \left(a_1 \frac{\Delta\rho}{\rho} + \frac{a_2}{\sqrt{8Re(f_r)}} \frac{\Delta\eta}{\eta} \right), \quad (5)$$

where ρ_{beam} is the mass density of the beam's material, $a_1 = 1.0553$, $a_2 = 3.7997$ are Maali's [23] parameters of the real part of the hydrodynamic function and $Re(f_r)$ is the Reynolds' number at the resonant frequency defined in Equation 6:

$$Re(f_r) = \frac{\pi b^2 \rho f_r}{4\eta}. \quad (6)$$

Under the same assumptions we get a similar expression for the quality factor Q shown in Equation 7:

$$\frac{\Delta Q}{Q} = -\frac{1}{2} \left(\frac{\Delta\rho}{\rho} + \frac{\Delta\eta}{\eta} \right). \quad (7)$$

Despite the fact that Equations 5 and 7 are valid for a very specific case (Euler-Bernoulli conditions), they are useful to give an insight in the parameters that play a role in the relative weight between $\Delta\rho$ and $\Delta\eta$ in both, the resonant frequency and the quality factor of a resonator.

In order to extract $\Delta\rho$ and $\Delta\eta$ in a more general case in terms of geometry (even if the Euler-Bernoulli conditions are not valid), we will assume that a first order approximation remains valid for small variations. Thus, Δf_r and ΔQ can be written as in Equations 8 and 9 where α_1 , α_2 , β_1 and β_2 can be considered constant since they depend on the geometry and technology of the resonator and on the predominant gas (N_2 in our case) but not on the gas present in a small amount:

$$\frac{\Delta f_r}{f_r} = \alpha_1 \frac{\Delta\rho}{\rho} + \beta_1 \frac{\Delta\eta}{\eta}, \quad (8)$$

$$\frac{\Delta Q}{Q} = \alpha_2 \frac{\Delta\rho}{\rho} + \beta_2 \frac{\Delta\eta}{\eta}. \quad (9)$$

Therefore if we are able to obtain such constants through calibration, then $\Delta\rho$ and $\Delta\eta$ are simply given by Equations 10 and 11, respectively:

$$\frac{\Delta\rho}{\rho} = \frac{1}{\alpha_1\beta_2 - \alpha_2\beta_1} \left(\beta_2 \frac{\Delta f_r}{f_r} - \beta_1 \frac{\Delta Q}{Q} \right), \quad (10)$$

$$\frac{\Delta\eta}{\eta} = \frac{1}{\alpha_1\beta_2 - \alpha_2\beta_1} \left(\alpha_1 \frac{\Delta Q}{Q} - \alpha_2 \frac{\Delta f_r}{f_r} \right). \quad (11)$$

In order to get the four parameters (α_1 , α_2 , β_1 and β_2) it is needed to measure Δf_r and ΔQ , for two different binary mixtures (nitrogen and either gas A or B) at a given concentration for each gas mixture (the corresponding $\Delta\rho$ and $\Delta\eta$ being determined using Equations 1 and 2). The system described by Equations 12 to 15 is then solved where the subscripts 'A' and 'B' designate the quantities of gases A and B respectively:

$$\frac{\Delta f_{r,A}}{f_r} = \alpha_1 \frac{\Delta \rho_A}{\rho} + \beta_1 \frac{\Delta \eta_A}{\eta}, \quad (12)$$

$$\frac{\Delta f_{r,B}}{f_r} = \alpha_1 \frac{\Delta \rho_B}{\rho} + \beta_1 \frac{\Delta \eta_B}{\eta}, \quad (13)$$

$$\frac{\Delta Q_A}{Q} = \alpha_2 \frac{\Delta \rho_A}{\rho} + \beta_2 \frac{\Delta \eta_A}{\eta}, \quad (14)$$

$$\frac{\Delta Q_B}{Q} = \alpha_2 \frac{\Delta \rho_B}{\rho} + \beta_2 \frac{\Delta \eta_B}{\eta}. \quad (15)$$

80 Which finally leads to the following equations to determine the four needed parameters:

$$\alpha_1 = \frac{\rho}{f_r} \frac{\Delta f_{r,A} \Delta \eta_B - \Delta f_{r,B} \Delta \eta_A}{\Delta \rho_A \Delta \eta_B - \Delta \rho_B \Delta \eta_A}, \quad (16)$$

$$\beta_1 = \frac{\eta}{f_r} \frac{\Delta f_{r,B} \Delta \rho_A - \Delta f_{r,A} \Delta \rho_B}{\Delta \rho_A \Delta \eta_B - \Delta \rho_B \Delta \eta_A}, \quad (17)$$

$$\alpha_2 = \frac{\rho}{Q} \frac{\Delta Q_A \Delta \eta_B - \Delta Q_B \Delta \eta_A}{\Delta \rho_A \Delta \eta_B - \Delta \rho_B \Delta \eta_A}, \quad (18)$$

$$\beta_2 = \frac{\eta}{Q} \frac{\Delta Q_B \Delta \rho_A - \Delta Q_A \Delta \rho_B}{\Delta \rho_A \Delta \eta_B - \Delta \rho_B \Delta \eta_A}. \quad (19)$$

This model fails when the influence of either the viscosity or the mass density is negligible in both the quality factor and the resonant frequency since the system becomes unsolvable. Typically one would only be able to measure the mass density as the sensors become smaller since the influence of the viscosity tends to decrease due to high resonant frequency and low quality factor.

85 4. Sensor Description

In order to validate the proposed method, a sensor not respecting the Euler Bernoulli condition $b \ll L$ has been chosen. This choice has been motivated in order to prove that even if the Equations 5 and 7 are not valid, the Equations 8 and 9 can be used (in the general case the expression of the parameters α_1 , α_2 , β_1 and β_2 as functions of the geometrical parameters and material properties of the resonant MEMS are different). For this study the sensor used had the following geometry: $h = 10 \mu\text{m}$, $b = L = 1 \text{mm}$. Figure 2a shows a picture of it. The details of the sensor manufacturing process, proof of its reversibility along with other details can be found in reference [13].

The working principle of both the actuation and the readout is illustrated in Figure 2b. An alternative current generated by an Agilent E5061B network analyzer passes through a conductive path located close to the edge of the top surface of the cantilever. In presence of a magnetic field \vec{B} , it induces a Lorentz force \vec{F} that makes the beam vibrate orthogonally to its plane (out-of-plane vibration). This was chosen, as opposed to in-plane vibration, because it strengthens the fluid/structure interaction [24] which is the basis of the principle of uncoated sensors. A first piezo-resistor then senses the strain close to the clamped part of the beam and another one is used as a reference to compensate for common mode variations such as a deformation of the piezo-resistor due to temperature. The readout is the signal at the middle point of the voltage divider bridge formed by the two piezo-resistors. This signal is then fed to the network analyzer to extract the measured phase (ϕ) spectrum (phase difference between the actuation signal and the readout signal). Finally a linear fit (ϕ_{fit}) of the phase close to the resonant frequency was applied to the phase curves as shown in Equation 20:

$$\phi_{fit} = c_0 + c_1 f, \quad (20)$$

105 where ϕ_{fit} is in radians, c_0 is its bias and c_1 its slope. This was done in order to extract both the resonant frequency and the quality factor as a function of time. Indeed, as explained by Boudjiet *et al.* [13], the equations to extract f_r and Q from such fit (ϕ_{fit}) are **Equations** 21 and 22, respectively:

$$f_r = -\frac{\frac{\pi}{2} + c_0}{c_1}, \quad (21)$$

$$Q = -\frac{c_1}{2} f_r. \quad (22)$$

5. Experiment

5.1. Measurements

110 With the previously described setup four gases (H_2 , He, CO_2 and CH_4) were used to validate the method. The microcantilevers are placed in a small gas chamber (total volume: 500 μL) under a controlled gas flow (100 $cm^3 \cdot min^{-1}$). Gas streams containing binary mixtures of the desired species (hydrogen or helium or carbon dioxide or methane) and nitrogen are fed to the chamber using bottles of gas (5% $H_2/95\% N_2$ or 100% He or 100% CO_2 or 10% $CH_4/90\% N_2$) and a set of mass-flow controllers (Brooks 5850S). They were introduced in three different concentrations 5%, 4% and 3% for 400 seconds each. N_2 was alternated in between each gas mixture for 400 seconds in order to compensate, if needed, for any considerable drift and to show the reversibility of the sensor. **Figures** 3a and 3b show respectively the resonant frequency and quality factor shifts for this experiment where the resonant frequency (f_{r,N_2}) and the quality factor in nitrogen (Q_{N_2}) are respectively 23.268 kHz and 500.

120 It can be noticed that for all of the four gases there is an associated shift in resonant frequency and quality factor (of roughly 100 ppm for Δf_r and 4000 ppm for ΔQ). Although studying this sensor's limit of detection is out of the scope of this article, it can be noticed that measuring smaller concentrations could be done with ease. In addition these curves are consistent with the full reversibility and fast response time (less than 1 min for 5% of H_2-N_2) of uncoated cantilevers in gas sensing with respect to typical sensors with sensitive film which is usually between 1 min and 10 min. The limiting factor in the response time in our experiment is the time that the gas takes to reach the sensor but one could potentially go below 1 min with a faster gas delivery. Moreover, there is nearly no drift (0.15Hz for Δf_r and 0.1 for ΔQ during 3 hours). The reproducibility of the measurements of both the resonant frequency and quality factor is not shown in the present paper but has already been shown in [13]. Finally, we notice that the trends in Δf_r and ΔQ are very similar for H_2 , He and CH_4 which are all lighter gases than N_2 . This could make it potentially difficult to differentiate each one of them by looking only at Δf_r and ΔQ . In such case, transforming the data to obtain the density and viscosity of each mixture can be quite useful, as presented in the next section.

5.2. Results

135 In order to test the proposed method, the model calibration was first done by using the mean value of the steps corresponding to CH_4 and He both at 5%. This allowed us to obtain the four parameters $\alpha_1 = -6.1 \times 10^{-3}$, $\beta_1 = -1.28 \times 10^{-4}$, $\alpha_2 = -4.4 \times 10^{-1}$, and $\beta_2 = -1.6 \times 10^{-1}$. The linear transform from **Equations** 10 and 11 was then applied to the measured Δf_r and ΔQ presented in **Figures** 3a and 3b. The resulting mass density and viscosity shifts are shown in **Figures** 4a and 4b.

140 We notice that, in one hand, the computed mass density varies roughly in the opposite way as the resonant frequency which is explained by the fact that $|\alpha_1| \gg |\beta_1|$ and $\alpha_1 < 0$. On the other hand, the computed viscosity varies in a completely different way than the resonant frequency or the quality factor. Moreover it can be seen that, despite the relatively low drift and noise in Δf_r and ΔQ with respect to the concentration jumps, in the case of the viscosity the noise and drift are much more noticeable.

145 Finally, the data points surrounded by a dashed box in **Figures** 4a and 4b were plot against each other along with the theory from **Figure** 1 for comparison in **Figure** 5. In this case, the small drifts were linearly compensated both in the density and the viscosity. For demonstration purposes, the angle bisector between two consecutive theoretical curves was used as frontier between the domains to assign one data point to a

gas mixture but this choice might need refining for other applications depending on their context. The slope of such domains frontiers are shown in [Table 3](#).

150 It can be noticed that, although no information about H_2 or CO_2 was given to the model (they were not used for the calibration) other than their corresponding Δf_r and ΔQ , the experimental points are remarkably close to their theoretical values which validates the model from [Section 3](#). The transform is, naturally, more accurate with the gases used for calibration (CH_4 and He in this case). It can also be seen that the different gases are relatively well distinguishable from one another apart from a few extreme
155 points corresponding to He that end up closer to the theoretical values for H_2 . **If we apply the method suggested in Section 2 to the mean values of each concentration step (dark red pentagons in Figure 5), we obtain the results shown in Table 4 where the first Columns 1 and 2 describe the binary mixture injected in the chamber, Column 7 describe the prediction of the binary gas mixture based on the value of the slope (Column 5) and the sign of $\Delta\rho$ (Column 6), The column 8 is the estimation of the gas concentration using the variation of the mass density (Column 3).**

160 **It can be seen that this method allows a very good discrimination of the different binary mixtures.** In addition, it can be noticed that we are able to predict the concentration of the mixture as well (in this case less than 3% of error for three of the mixtures and a maximum of 12% of error for CO_2). Nevertheless it seems that how accurate the results are depends on how similar a gas-mixture is from the gases used in the
165 calibration. Indeed, since H_2 is more similar to He than CO_2 is to either CH_4 or He, a better prediction of the concentration of H_2 than of CO_2 is obtained.

6. Optimizing the Calibration Procedure

In order to understand better the robustness of the proposed method we developed a simulator that, from the theoretical values of both the viscosity and the mass density for the different gases as well as from the
170 theoretical parameters α_1 , α_2 , β_1 and β_2 from [Section 3](#) (assuming a cantilever respecting Euler-Bernoulli conditions), generates the associated shifts pair Δf_r and ΔQ as a function of time. A white Gaussian noise is then added to the model. Since the goal in this section is to optimize the calibration procedure, the mean distance between a simulated data point and its theoretical value ([Equation 23](#)) is used as error metric:

$$\epsilon = \frac{1}{N} \sum_{i=1}^N \sqrt{\left(\frac{\Delta\rho_i^{exp} - \Delta\rho_i^{th}}{\rho_{N_2}}\right)^2 + \left(\frac{\Delta\eta_i^{exp} - \Delta\eta_i^{th}}{\eta_{N_2}}\right)^2}, \quad (23)$$

175 where N is the total number of simulated data points. To limit biasing the error computation and covering more parts of the density viscosity plane, two more gases, CO and O_2 , were added to the simulation.

6.1. Calibration Concentration

The objective of this part is to determine weather it is better to calibrate with a high concentration or a low concentration (keeping in mind that the concentrations must remain small for the model to hold). To test this, several simulations were ran calibrating with He and CH_4 at different concentration pairs. The
180 resulting error values are shown in [Figure 6](#).

It can be noticed that the mean error decreases as higher concentrations to calibrate are used. Therefore, the calibration should be done with concentrations as big as possible as long as the small variation assumption holds.

6.2. Choice of the Two Gas Mixtures

185 Having studied the calibration dependency on the concentration, there is left to test which pair of gas mixtures is more appropriate for the calibration. In order to do so, several simulations were ran calibrating this time with each pair of gas mixtures at a fixed distance from the origin. The points used for calibration in this set of simulations are marked by a red star in [Figure 7-a](#). For all the possible pair of points (corresponding to the gas pair for calibration) the corresponding error was plotted against the angle θ between the theoretical

190 curves (Figure 7-b) of the corresponding mixtures. As an example, the angle between the curves of the mixtures CO₂-N₂ and CH₄-N₂ is shown in Figure 7-a.

It can be noticed (Figure 7-b) that most pairs of mixtures used to calibrate have an error below 0.4 except for the combinations He/H₂, He/CO₂ and O₂/CH₄. These three combinations, as shown in Figures 7 a and b, correspond to the curves that are almost aligned (θ close to either 0° or 180°). This allows to conclude that the closer to collinearity the curves of the mixtures used for the calibration are, the worse the performance of the method is. This can be explained by the fact that, in order to compute the four parameters α_1 , α_2 , β_1 and β_2 , it is required to divide by $\Delta\rho_A\Delta\eta_B - \Delta\rho_B\Delta\eta_A$ (Equations 16 to 19). However, it can be shown that for two mixtures A and B for which the curves are nearly collinear, this value is close to zero which causes that a small variation due to the noise can lead to a significantly different value of the parameters.

Conclusion

A simple method to extract both the gas mass density and the gas viscosity from the measurement of both the quality factor and the resonant frequency of a microresonator without sensitive coating has been presented. In a gas of reference (which can be a mixture of gas and which is nitrogen in the presented measurements) if one gas appears it is possible with the determination of the two physical properties of gas (mass density and viscosity), to know which gas has appeared and the concentration of this gas. The proposed method can be used in a mixture of three or more mixture of gases only if it is known that only one concentration of the gas is modified the proportion of the other ones staying stable. This could be useful in some industries to detect gas leakages for example. The main advantages of such method are: (1) the smaller time response compared to the one of chemical sensors using sensitive layer, (2) the possibility to discriminate between different gases and to estimated the gas concentration with only one sensor, (3) the aging and reversibility of such sensors are very good due to the absence of sensitive coating. The presented method has been validated with four different gas mixtures using a silicon microcantilever. The discrimination of the four gases has been achieved and the estimation of the gas concentration has been obtained with less than 3% of error for three gases and less than 12% for the last one. This has been performed using a calibration step with two gases at a fixed concentration. The impact of this calibration step has been studied and a general way to choose the gases and the concentration for the calibration has been established.

Acknowledgement

220 This research was done thanks to the contest *Programme d'Investissements d'Avenir* of the French Government under the supervision of the French National Radioactive Waste Management Agency (ANDRA). Special thanks to Thierry Leïchlé, Laurent Mazenq and Liviu Nicu from LAAS/CNRS for fabricating the silicon microsensors used in this study.

References

- 225 [1] G. Korotcenkov, B. Cho, Instability of metal oxide-based conductometric gas sensors and approaches to stability improvement (short survey) 156 (2) (2011) 527–538. doi:10.1016/j.snb.2011.02.024.
URL <http://linkinghub.elsevier.com/retrieve/pii/S0925400511001353>
- [2] A.-C. Romain, P. André, J. Nicolas, Three years experiment with the same tin oxide sensor arrays for the identification of malodorous sources in the environment 84 (2) (2002) 271–277. doi:10.1016/S0925-4005(02)00036-9.
230 URL <http://linkinghub.elsevier.com/retrieve/pii/S0925400502000369>
- [3] A. Romain, J. Nicolas, Long term stability of metal oxide-based gas sensors for e-nose environmental applications: An overview 146 (2) (2010) 502–506. doi:10.1016/j.snb.2009.12.027.
URL <http://linkinghub.elsevier.com/retrieve/pii/S0925400509009630>
- 235 [4] R. K. Sharma, P. C. Chan, Z. Tang, G. Yan, I.-M. Hsing, J. K. Sin, Investigation of stability and reliability of tin oxide thin-film for integrated micro-machined gas sensor devices 81 (1) (2001) 9–16. doi:10.1016/S0925-4005(01)00920-0.
URL <http://linkinghub.elsevier.com/retrieve/pii/S0925400501009200>

- [5] W. Göpel, New materials and transducers for chemical sensors 18 (1) (1994) 1–21. doi:10.1016/0925-4005(94)87049-7. URL <http://linkinghub.elsevier.com/retrieve/pii/0925400594870497>
- [6] N. Yamazoe, New approaches for improving semiconductor gas sensors 5 (1) (1991) 7–19. doi:10.1016/0925-4005(91)80213-4. URL <http://linkinghub.elsevier.com/retrieve/pii/0925400591802134>
- [7] M. Padilla, A. Perera, I. Montoliu, A. Chaudry, K. Persaud, S. Marco, Drift compensation of gas sensor array data by orthogonal signal correction 100 (1) (2010) 28–35. doi:10.1016/j.chemolab.2009.10.002. URL <http://linkinghub.elsevier.com/retrieve/pii/S0169743909001877>
- [8] A. Vergara, S. Vembu, T. Ayhan, M. A. Ryan, M. L. Homer, R. Huerta, Chemical gas sensor drift compensation using classifier ensembles 166-167 (2012) 320–329. doi:10.1016/j.snb.2012.01.074. URL <http://linkinghub.elsevier.com/retrieve/pii/S0925400512002018>
- [9] F. Hossein-Babaei, V. Ghafarina, Compensation for the drift-like terms caused by environmental fluctuations in the responses of chemoresistive gas sensors 143 (2) (2010) 641–648. doi:10.1016/j.snb.2009.10.006. URL <http://linkinghub.elsevier.com/retrieve/pii/S0925400509007746>
- [10] R. Rosario, R. Mutharasan, Piezoelectric excited millimeter sized cantilever sensors for measuring gas density changes 192 (2014) 99–104. doi:10.1016/j.snb.2013.10.017. URL <http://linkinghub.elsevier.com/retrieve/pii/S0925400513012033>
- [11] S. Tétin, B. Caillard, F. Ménil, H. Debéda, C. Lucat, C. Pellet, I. Dufour, Modeling and performance of uncoated microcantilever-based chemical sensors 143 (2) (2010) 555–560. doi:10.1016/j.snb.2009.09.062. URL <http://linkinghub.elsevier.com/retrieve/pii/S0925400509007655>
- [12] M. Boudjiet, V. Cuisset, C. Pellet, J. Bertrand, I. Dufour, Preliminary results of the feasibility of hydrogen detection by the use of uncoated silicon microcantilever-based sensors 39 (35) (2014) 20497–20502. doi:10.1016/j.ijhydene.2014.03.228. URL <http://linkinghub.elsevier.com/retrieve/pii/S0360319914009562>
- [13] M. Boudjiet, J. Bertrand, F. Mathieu, L. Nicu, L. Mazenq, T. Leïchlé, S. Heinrich, C. Pellet, I. Dufour, Geometry optimization of uncoated silicon microcantilever-based gas density sensors 208 (2015) 600–607. doi:10.1016/j.snb.2014.11.067. URL <http://linkinghub.elsevier.com/retrieve/pii/S0925400514014476>
- [14] B. A. Bircher, L. Duempelmann, K. Renggli, H. P. Lang, C. Gerber, N. Bruns, T. Braun, Real-time viscosity and mass density sensors requiring microliter sample volume based on nanomechanical resonators 85 (18) (2013) 8676–8683. doi:10.1021/ac4014918. URL <http://pubs.acs.org/doi/10.1021/ac4014918>
- [15] K. Igarashi, K. Kawashima, T. Kagawa, Development of simultaneous measurement system for instantaneous density, viscosity and flow rate of gases 140 (1) (2007) 1–7. doi:10.1016/j.sna.2007.06.017. URL <http://linkinghub.elsevier.com/retrieve/pii/S0924424707004931>
- [16] J. Lötters, E. van der Wouden, J. Groenesteijn, W. Sparreboom, T. Lammerink, R. Wiegerink, Integrated multi-parameter flow measurement system, IEEE, 2014, pp. 975–978. doi:10.1109/MEMSYS.2014.6765806. URL <http://ieeexplore.ieee.org/document/6765806/>
- [17] D. Seibt, S. Herrmann, E. Vogel, E. Bich, E. Hassel, Simultaneous measurements on helium and nitrogen with a newly designed viscometerdensimeter over a wide range of temperature and pressure 54 (9) (2009) 2626–2637. doi:10.1021/je900131q. URL <http://pubs.acs.org/doi/abs/10.1021/je900131q>
- [18] W. Sutherland, LII. *The viscosity of gases and molecular force* 36 (223) (1893) 507–531. doi:10.1080/14786449308620508. URL <http://www.tandfonline.com/doi/abs/10.1080/14786449308620508>
- [19] R. S. Brokaw, Predicting transport properties of dilute gases 8 (2) (1969) 240–253. doi:10.1021/i260030a015. URL <http://pubs.acs.org/doi/abs/10.1021/i260030a015>
- [20] C. R. Wilke, A viscosity equation for gas mixtures 18 (4) (1950) 517–519. doi:10.1063/1.1747673. URL <http://aip.scitation.org/doi/10.1063/1.1747673>
- [21] J. E. Sader, Frequency response of cantilever beams immersed in viscous fluids with applications to the atomic force microscope 84 (1) (1998) 64–76. doi:10.1063/1.368002. URL <http://aip.scitation.org/doi/10.1063/1.368002>
- [22] J. W. M. Chon, P. Mulvaney, J. E. Sader, Experimental validation of theoretical models for the frequency response of atomic force microscope cantilever beams immersed in fluids 87 (8) (2000) 3978–3988. doi:10.1063/1.372455. URL <http://aip.scitation.org/doi/10.1063/1.372455>
- [23] A. Maali, C. Hurth, R. Boisgard, C. Jai, T. Cohen-Bouhacina, J.-P. Aimé, Hydrodynamics of oscillating atomic force microscopy cantilevers in viscous fluids 97 (7) (2005) 074907. doi:10.1063/1.1873060. URL <http://aip.scitation.org/doi/10.1063/1.1873060>
- [24] I. Dufour, E. Lemaire, B. Caillard, H. Debéda, C. Lucat, S. Heinrich, F. Josse, O. Brand, Effect of hydrodynamic force on microcantilever vibrations: Applications to liquid-phase chemical sensing, *Sensors and Actuators B: Chemical* 192 (2014) 664–672. doi:10.1016/j.snb.2013.10.106. URL <https://linkinghub.elsevier.com/retrieve/pii/S0925400513013087>
- [25] A. J. Zuckerwar, *Handbook of the Speed of Sound in Real Gases.*, Elsevier, 2002, OCLC: 476075880. URL <http://public.eblib.com/choice/publicfullrecord.aspx?p=299110>
- [26] Engineering ToolBox | <https://www.engineeringtoolbox.com/> (November 2017).
- [27] Gas encyclopedia air liquide | <https://encyclopedia.airliquide.com/> (November 2017). URL <https://encyclopedia.airliquide.com/>

Figures and Tables

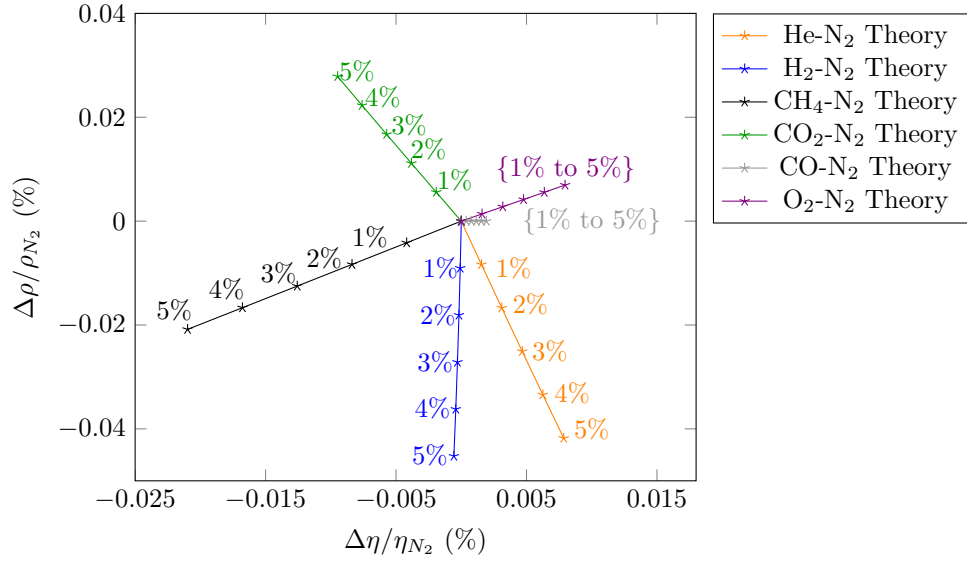


Figure 1: Relative mass density variation vs. relative viscosity variation with respect to N_2 for different gases and different concentrations at $25^\circ C$ and atmospheric pressure

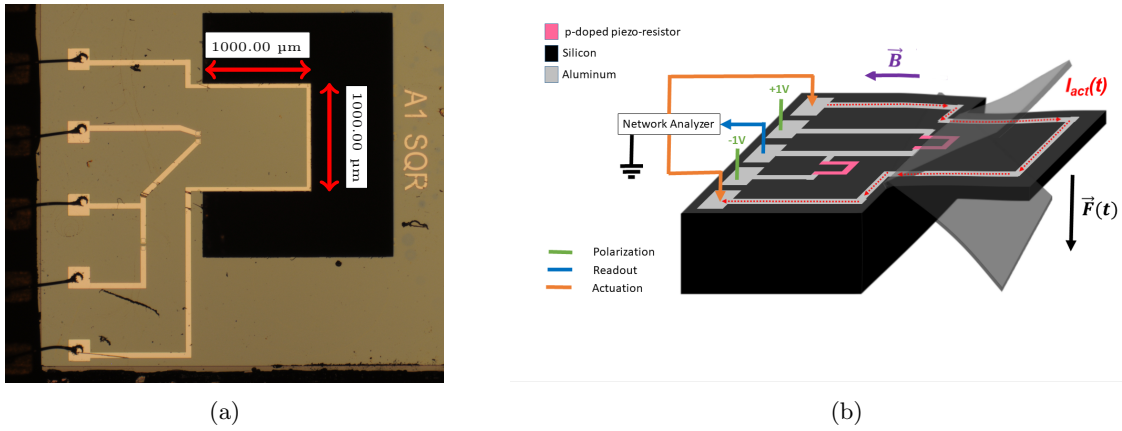
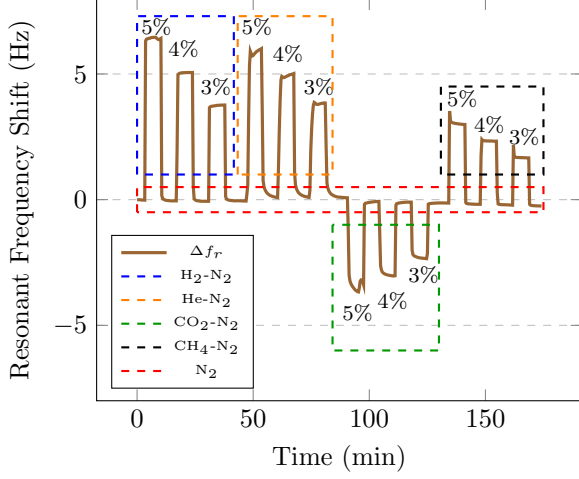
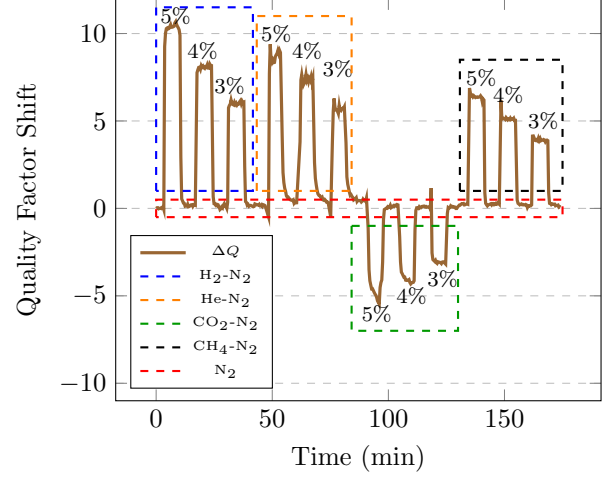


Figure 2: Silicon electromagnetically actuated sensor with piezo-resistive readout used in this study: (a) picture ($L = 1$ mm, $b = 1$ mm, $h = 10$ μm), (b) schematic illustrating both the actuation and the read-out

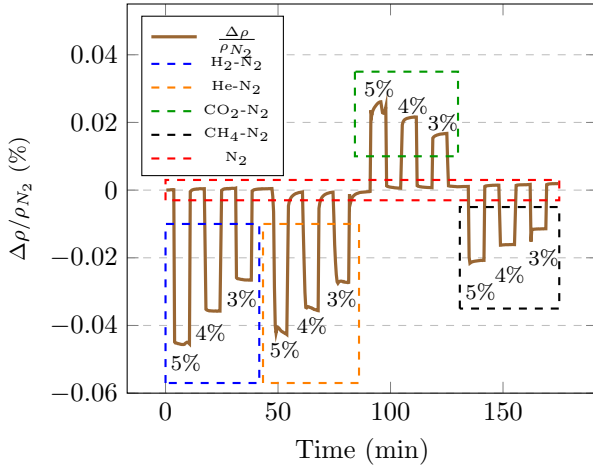


(a) Resonant frequency shift

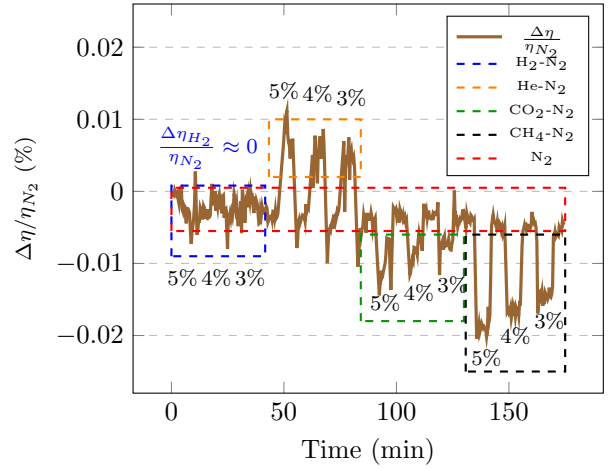


(b) Quality factor shift

Figure 3: Shifts for different gas mixtures at different concentrations (5%, 4% and 3%)



(a) Mass density shift computed using the data from **Figures 3a** and **3b** using Equation 10



(b) Viscosity shift computed using the data from **Figures 3a** and **3b** and Equation 11

Figure 4: Computed shifts for different gas mixtures at different concentrations (5%, 4% and 3%) where $\alpha_1 = 6.1 \times 10^{-3}$, $\beta_1 = 1.28 \times 10^{-4}$, $\alpha_2 = 4.4 \times 10^{-1}$, $\beta_2 = 1.6 \times 10^{-1}$

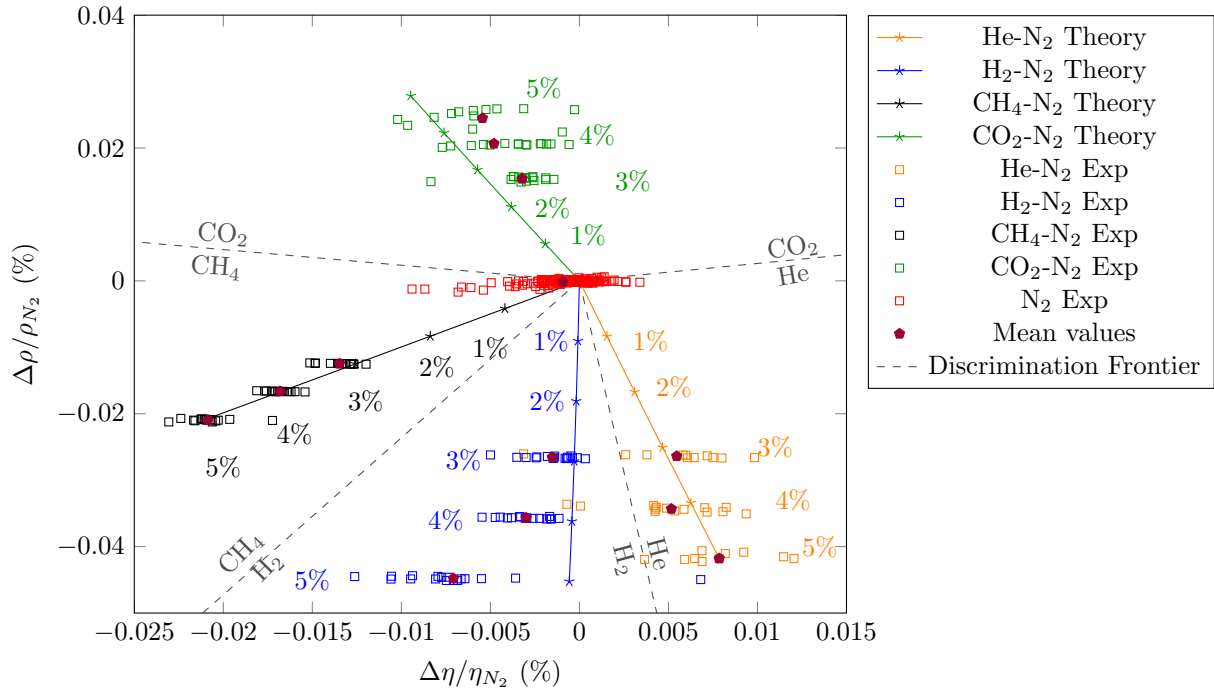


Figure 5: Simultaneous measurements of both the mass density and the viscosity using the data presented in [Figures 4a](#) and [4b](#)

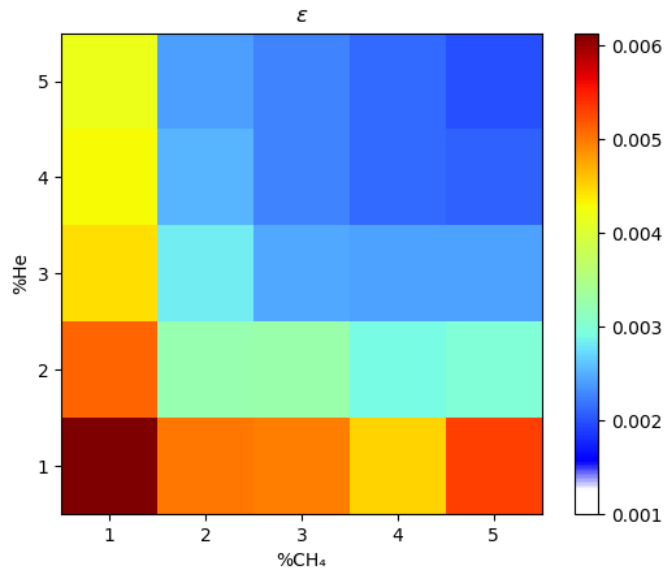


Figure 6: Mean error (equation 23) for different concentration pairs using CH₄ and He to calibrate

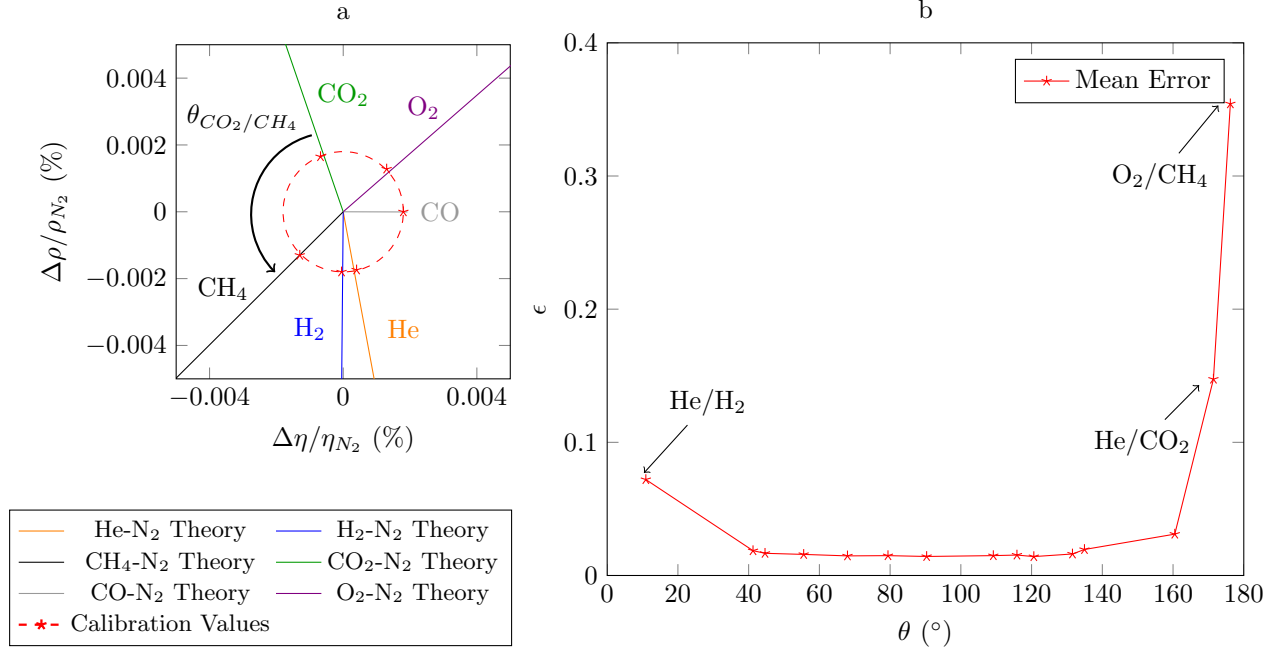


Figure 7:

- a: Explanation of the calibration at a fixed distance from the origin and definition of θ , the angle between the theoretical density-viscosity curves for two mixtures.
- b: Mean error of a calibration at a fixed distance from the origin as a function of the angle between the theoretical density-viscosity curves as shown in [Figure 7-a](#) of the pair of gas mixtures used in the calibration

Table 1: Physical properties of common gases[25, 26, 27]

Gas	Mass Density ($\text{kg} \cdot \text{m}^{-3}$) 1.015 bar, 15°C	Viscosity ($\mu\text{Pa} \cdot \text{s}$) 1.015 bar, 0°C	Thermal Conductivity ($\text{mW} \cdot \text{m}^{-1} \cdot \text{K}^{-1}$) 1.015 bar, 0°C	Speed of Sound $\text{m} \cdot \text{s}^{-1}$ 1.015 bar, 20°C
CO ₂	1.87	13.7	14.7	267
O ₂	1.35	19.1	24.4	326
Air	1.22	17.2	24.4	343
CO	1.18	16.5	24.7	336
N ₂	1.18	16.6	24.0	349
CH ₄	0.68	10.1	30.6	446
He	0.17	18.7	146.2	1007
H ₂	0.09	8.4	176.2	1270

Table 2: Theoretical values of the slope of the curves of [Figure 1](#) and sensitivities of both density and viscosity for different gases mixtures

Gas Mixture	$\frac{\Delta\rho}{\rho_{N_2}} \frac{\eta_{N_2}}{\Delta\eta}$ (x1)	$\frac{\Delta\rho}{x_G \eta_{N_2}}$ (x10 ⁻³ /%)	$\frac{\Delta\eta}{x_G \eta_{N_2}}$ (x10 ⁻³ /%)	Sign of $\Delta\rho$
CO ₂ -N ₂	-2.94	5.6	1.9	+
O ₂ -N ₂	0.872	1.39	1.6	+
He-N ₂	-5.32	8.4	1.6	-
CO-N ₂	-0.0027	0.001	0.38	-
CH ₄ -N ₂	0.99	4.2	4.2	-
H ₂ -N ₂	80.7	9.1	0.11	-

Table 3: Value of the slope of the frontier between domains

Frontier	H ₂ /He	CO ₂ /CH ₄	He/CO ₂	CH ₄ /H ₂
Slope (x1)	-11.5	-0.236	0.263	2.3560

Table 4: Summary of the method presented in [Section 2](#) applied to the mean values of viscosity and density for each concentration (dark red pentagons in [Figure 5](#))

Used Mixture		Measured				Predicted	
Gases	x_G	$\frac{\Delta\rho}{\rho_{N_2}}$	$\frac{\Delta\eta}{\eta_{N_2}}$	Slope	Sign of $\Delta\rho$	Gases	x_G Using $\frac{\Delta\rho}{\rho_{N_2}}$
	(%)	(x10 ⁻² %)	(x10 ⁻² %)	(x1)			(%)
N ₂ -CO ₂	3	1.54	-0.322	-4.78	+	N ₂ -CO ₂	2.8
	4	2.07	-0.480	-4.31	+	N ₂ -CO ₂	3.7
	5	2.45	-0.545	-4.5	+	N ₂ -CO ₂	4.4
N ₂ -CH ₄	3	-1.25	-1.35	0.926	-	N ₂ -CH ₄	3.0
	4	-1.66	-1.68	0.988	-	N ₂ -CH ₄	4.0
	5	-2.10	-2.09	1.00	-	N ₂ -CH ₄	5.0
N ₂ -He	3	-2.64	0.546	-4.83	-	N ₂ -He	3.1
	4	-3.43	0.517	-6.63	-	N ₂ -He	4.0
	5	-4.15	0.667	-6.22	-	N ₂ -He	5.0
N ₂ -H ₂	3	-2.66	-0.152	17.5	-	N ₂ -H ₂	2.9
	4	-3.57	-0.299	11.9	-	N ₂ -H ₂	4.0
	5	-4.48	-0.707	6.33	-	N ₂ -H ₂	5.0